

ORIGINAL ARTICLE

Global and Parallel Cortical Processing Based on Auditory Gamma Oscillatory Responses in Humans

Mariko Tada^{1,2}, Kenji Kirihara¹, Yohei Ishishita³, Megumi Takasago⁴, Naoto Kunii⁴, Takanori Uka⁵, Seiji Shimada⁴, Kenji Ibayashi⁴, Kensuke Kawai³, Nobuhito Saito⁴, Daisuke Koshiyama¹, Mao Fujioka¹, Tsuyoshi Araki¹ and Kiyoto Kasai^{1,2}

¹Department of Neuropsychiatry, Graduate School of Medicine, The University of Tokyo, 7-3-1 Hongo, Bunkyo-ku, Tokyo 113-8655, Japan, ²International Research Center for Neurointelligence (WPI-IRCN), UTIAS, The University of Tokyo, 7-3-1 Hongo, Bunkyo-ku, Tokyo 113-0033, Japan, ³Department of Neurosurgery, Jichi Medical University, 3311-1 Yakushiji, Shimotsuke, Tochigi 329-0498, Japan, ⁴Department of Neurosurgery, Graduate School of Medicine, The University of Tokyo, 7-3-1 Hongo, Bunkyo-ku, Tokyo 113-8655, Japan and ⁵Department of Integrative Physiology, Graduate School of Medicine, University of Yamanashi, 1110 Shimokato, Chuo, Yamanashi 409-3898, Japan

Address correspondence to email: tadam@g.ecc.u-tokyo.ac.jp

Abstract

Gamma oscillations are physiological phenomena that reflect perception and cognition, and involve parvalbumin-positive γ -aminobutyric acid-ergic interneuron function. The auditory steady-state response (ASSR) is the most robust index for gamma oscillations, and it is impaired in patients with neuropsychiatric disorders such as schizophrenia and autism. Although ASSR reduction is known to vary in terms of frequency and time, the neural mechanisms are poorly understood. We obtained high-density electrocorticography recordings from a wide area of the cortex in 8 patients with refractory epilepsy. In an ASSR paradigm, click sounds were presented at frequencies of 20, 30, 40, 60, 80, 120, and 160 Hz. We performed time-frequency analyses and analyzed intertrial coherence, event-related spectral perturbation, and high-gamma oscillations. We demonstrate that the ASSR is globally distributed among the temporal, parietal, and frontal cortices. The ASSR was composed of time-dependent neural subcircuits differing in frequency tuning. Importantly, the frequency tuning characteristics of the late-latency ASSR varied between the temporal/frontal and parietal cortex, suggestive of differentiation along parallel auditory pathways. This large-scale survey of the cortical ASSR could serve as a foundation for future studies of the ASSR in patients with neuropsychiatric disorders.

Key words: auditory steady-state response, electrocorticography (ECoG), gamma oscillation, high-frequency oscillation (HFO), intertrial coherence (ITC)

Introduction

Gamma oscillations have attracted attention due to their role in perception and cognition, and their association with inhibitory parvalbumin (PV)-positive γ -aminobutyric acid (GABA)-ergic interneurons (Cardin et al. 2009; Sohal et al. 2009; Cardin 2016). Abnormal gamma oscillations are consistently detected in subjects with neuropsychiatric disorders such as schizophrenia and autism spectrum disorder (Uhlhaas and Singer 2010; Sun et al. 2011). Specifically, a reduction in the gamma-band auditory steady-state response (ASSR), a measure of oscillatory responses to periodic auditory stimuli (Galambos et al. 1981), is the most robust finding linking gamma oscillations with schizophrenia (Thuné et al. 2016; Tada et al. 2019) and animal disease models (Sivarao 2015; Sivarao et al. 2016; Kozono et al. 2019).

Despite the crucial role that gamma oscillations play in cognitive processing and cognitive disorders, the precise location of gamma-band ASSR in the human brain remains controversial (Farahani et al. 2019). Previous noninvasive magnetoencephalography (MEG) studies have shown that gamma-band ASSR is localized in the superior temporal plane, presumably corresponding to the primary auditory cortex (A1; Herdman et al. 2003; Draganova et al. 2008). Brugge et al. (2009) used a depth electrode to observe gamma-band ASSR in postero-medial Heschl's gyrus, near A1. In contrast to these conventional studies, some previous reports showed that potential sources of the ASSR are not limited to the auditory cortex. Source estimation using an independent component analysis of electroencephalography (EEG) data showed a widely distributed network of the ASSR not only in the temporal cortex, but also in the frontal cortex and subcortical regions (Farahani et al. 2017). However, findings have varied according to the analytic methods. In an updated localization study using group-ICA for more accurate source reconstruction of the same data found in Farahani et al. (2017), the frontal cortex was not confirmed as the source; instead it was the parietal cortex (Farahani et al. 2019). The precision of the signal localization may have been limited by the low spatial resolution of the EEG, in turn due to signal attenuation by the skull (Cohen and Cuffin 1983). Therefore, whether there are cortical sources of the ASSR other than the auditory cortex is still a matter of debate. ASSR reduction is a robust finding in various neuropsychiatric disorders, and is often associated with symptom severity or cognitive dysfunction, rather than merely auditory dysfunction (Tada et al. 2016; Koshiyama et al. 2018; Zhou et al. 2018). Thus, impairments in cortical sources outside the auditory cortex may affect ASSR reduction in patients.

Different frequency rhythms are believed to have different generation mechanisms and functions in the brain (Hutcheon and Yarom 2000; Kopell et al. 2010; Whittington et al. 2019). For example, a rodent study showed that PV-positive neurons are associated with gamma-band oscillation (typically 30–100 Hz), whereas somatostatin (SOM)-positive neurons are associated with beta-band oscillation (typically 13–30 Hz; Chen et al. 2017). In previous clinical studies, ASSR reduction in patients with schizophrenia was achieved at 40 but not 20 Hz (Uhlhaas and Singer 2010). High-frequency oscillations (60–200 Hz), which are easier to detect using electrocorticography (ECoG) compared with scalp EEG, have been observed in a variety of functional brain systems (Crone et al. 2006). Therefore, exploring wider oscillation frequencies in addition to the gamma band is important.

In this study, we investigated how the frequency and temporal characteristics of the ASSR varied across cortical regions in humans. The ASSR is believed to be composed of an early-transient and late-sustained component that have different neural underpinnings (Pantev et al. 1993, 1996; Ross et al. 2002; Ross and Pantev 2004; Ding and Simon 2009). Several previous clinical studies investigated the time course of ASSR (O'Donnell et al. 2004; Light et al. 2006; Wilson et al. 2007, 2008; Hamm et al. 2011; Rojas et al. 2011; Tada et al. 2016); specifically, a late-latency ASSR equivalent to the sustained component was more reduced in patient groups. We used ECoG that could detect local signals (Dubey and Ray 2019) from a large cortical area spanning the bilateral temporal, frontal, and parietal cortices, to precisely determine the intracranial location and topographical organization of the ASSR and its frequency and time dependence.

Materials and Methods

Participants

We recorded ECoG from 11 patients with refractory epilepsy who underwent subdural electrode implantation for diagnostic purposes (identification of epileptic foci and localization of functional brain areas) at the University of Tokyo Hospital between June 2014 and February 2017. The participants were aged between 18 and 58 years (mean age: 32.3, standard deviation [SD]: 13.6) and had left hemisphere language dominance. No patient had a low premorbid intelligence quotient (IQ < 70). Participants were screened using the Mini-International Neuropsychiatric Interview (Sheehan et al. 1998), which was conducted by an experienced psychiatrist, to rule out psychiatric disorders. One patient was excluded due to a diagnosis of autism spectrum disorder. Two additional patients were excluded due to definite epileptiform discharges which were hard to exclude by the off-line analysis on the continuous ECoG data. As a result, our analyses were restricted to 8 patients (5 males and 3 females). The clinical characteristics of the participants are presented in Table 1. Prior to enrollment, audiometric testing was used to confirm that all participants were able to detect 1000 and 4000 Hz tones at 30 dB, as per the criteria of the Oto-Rhino-Laryngological Society of Japan for general medical examinations. This study was approved by the institutional review board of the University of Tokyo Hospital (No. 1797). Written informed consent was obtained from all patients, and from the families of the younger participants, following a detailed explanation of the study. The participants were the same as in previously reported studies (Ishishita et al. 2019; Takasago et al. 2020).

Electrode Implantation and Data Acquisition

Electrode implantation was conducted in a similar manner to previous studies (Kunii et al. 2013a, 2013b). We used grid-type subdural electrodes, which consisted of silastic sheets embedded with platinum electrodes (Unique Medical). Two types of electrode sheets, a conventional sheet with a 3-mm diameter electrode and 10-mm interelectrode interval (center to center), or a high-density sheet with a 1.5-mm diameter electrode and 5-mm interelectrode interval (center to center) covered the lateral surface of the frontal, temporal, and parietal lobes. It was important to perform precise functional mapping in the left hemisphere to avoid resection of the language area during

Table 1 Demographic characteristics of the study participants

No.	Age (years)/sex	Duration of epilepsy (years)	Electrode coverage	Epileptic foci	Etiology and MRI findings	AED
1	43/M	23	Bilateral FT	Left lateral & medial T	No lesion	LTG, GBP, CBZ
2	20/M	2	Bilateral FTP	Bilateral T	No lesion	LEV, CLB
3	33/F	20	Bilateral FTP	Right lateral and medial T	Heterotopia in left lateral ventricle	LTG, CBZ, PHT, CBZ
4	58/F	49	Left FTP	Left lateral and medial T	Old CI of left basal ganglia	LEV, LTG, ZNS
5	20/F	12	Left FTP	Left lateral and medial T	No lesion	LEV, LTG, VPA, ZNS
6	36/M	18	Bilateral FTP	Left lateral T	No lesion	TPM, VPA, CLB
7	18/M	10	Bilateral FTP	Right O	Right O ganglioglioma	LEV, LTG, CBZ
8	30/M	14	Bilateral FTP	Right lateral T	No lesion	LEV, TPM, GBP

Abbreviations: AED: anti-epileptic drug; CBZ: carbamazepine; CI: cerebral infarction; CLB: clobazam; F/O/P/T: frontal/occipital/parietal/temporal lobe; GBP: gabapentin; LEV: levetiracetam; LTG: lamotrigine; MRI: magnetic resonance imaging; PHT: phenytoin; TPM: topiramate; VPA: valproate; ZNS: zonisamide.

epilepsy surgery. Therefore, we used smaller (high-density) electrodes for the dominant hemisphere, while standard electrodes were used in the nondominant hemisphere. Electrode locations were identified by a postimplantation-computed tomography scan registered to a preimplantation MRI scan based on the mutual information method, using Dr-View software (Infocom Corp.) for the Linux operating system. Three-dimensional (3D) brain surfaces with subdural electrodes were reconstructed using Real INTAGE software (Cybernet Systems, Ltd.). For group-level analysis, each electrode location was transformed to Montreal Neurological Institute (MNI) coordinates using the parameters generated during normalization of 3D MRI data with SPM8 software (<http://www.fil.ion.ucl.ac.uk/spm>). We identified Brodmann areas (BAs) from MNI coordinates using the MNI2TAL conversion tool (Papademetris et al., <http://www.bioimagesuite.org>). MNI-to-Talairach mapping and BA localization were based on previously described methods (Lacadie et al. 2008). Electrodes in the occipital lobe were excluded from this analysis.

ECoG data were digitally sampled and recorded at 2000 Hz using a multichannel EEG system (EEG 1200; Nihon Kodan Corp.). The hardware band-pass filter was set to 0.09–600 Hz. A reference electrode was placed on the inner surface of the dura mater over the parietal lobe.

Auditory Stimuli and Procedures

The ASSR paradigm was employed as described previously (Tada et al. 2016). Briefly, participants were seated on a bed with a reclining backrest in a quiet, electrically shielded room and instructed to relax with their eyes open. Auditory stimuli were presented binaurally through inserted earphones (Multi Trigger System; Medical Try System). The auditory stimuli were click sounds (80 dB and 1 ms) presented in 500-ms trains at frequencies of 20, 30, 40, 60, 80, 120, and 160 Hz. Click sound trains were presented at each frequency in a single block containing 120 sequences. The intertrain interval was 500 ms.

Data Analyses

We used the EEGLAB Matlab toolbox (Delorme and Makeig 2004) to perform offline analyses. We excluded 3 bad channels that were affected by excess epileptic discharge and artifacts. A

total of 1175 electrodes in the left hemisphere and 378 in the right hemisphere were included in the analysis. A high-pass filter (1 Hz) and notch filter (50, 150 Hz) were applied to the EEG data to remove artifacts. EEG data were segmented from –250 to 750 ms relative to the stimulus onset. The mean of the prestimulus baseline was subtracted for baseline correction. Epochs exceeding $\pm 1000 \mu\text{V}$ at any electrode were rejected. The number of artifact-free epochs did not differ significantly among stimulus frequencies (one-way analysis of variance [ANOVA], $F_{6,48} = 1.16$, $P = 0.34$). The mean (\pm SD) numbers of epochs for each stimulus frequency were as follows: 20 Hz: 111 ± 7 ; 30 Hz: 111 ± 3 ; 40 Hz: 112 ± 6 ; 60 Hz: 116 ± 3 ; 80 Hz: 109 ± 9 ; 120 Hz: 114 ± 5 ; and 160 Hz: 112 ± 5 .

We performed time-frequency analyses via short-term Fourier transformation, and then calculated intertrial coherence (ITC) and event-related spectral perturbation (ERSP) in the same manner as our previous study (Tada et al. 2016), as well as high-gamma activity (HGA). HGA was extracted as the average ERSP within the frequency range of 70–200 Hz at each time point, excluding frequencies around the ASSR stimulus frequency (80 ± 5 , 120 ± 5 , and 160 ± 5 Hz). ITC indicates the phase consistency across trials, and ranges between 0 (random phase across trials) and 1 (identical phase across trials). For ITC calculations, short-term Fourier transformation (Hanning window) was performed in each epoch using the EEGLAB function (`timef()`), as referred to in a previous report (Roach and Mathalon 2008). ERSP indicates event-related changes in power relative to a prestimulus baseline. HGA is a proxy for multiunit activity (Ray et al. 2008). Decreases in ITC and ERSP are often reported in patients with schizophrenia (Kwon et al. 1999; Light et al. 2006, 2017; Spencer et al. 2008; Brenner et al. 2009; Kirihara et al. 2012; Thuné et al. 2016). We also measured evoked power in addition to ITC and ERSP, because evoked power is more robust to noise. Evoked power was calculated using a short-term Fourier transformation (Hanning window) after averaging the data across trials for each electrode.

We calculated the mean ITC and ERSP at all electrode sites by averaging the data over the first 500 ms within a trial (0–500 ms) for each frequency range (20 Hz: 16–25; 30 Hz: 26–35; 40 Hz: 36–45; 60 Hz: 56–65; 80 Hz: 76–85; 120 Hz: 116–125; and 160 Hz: 156–165). The mean HGA was calculated in a similar way, but independent of ASSR frequency.

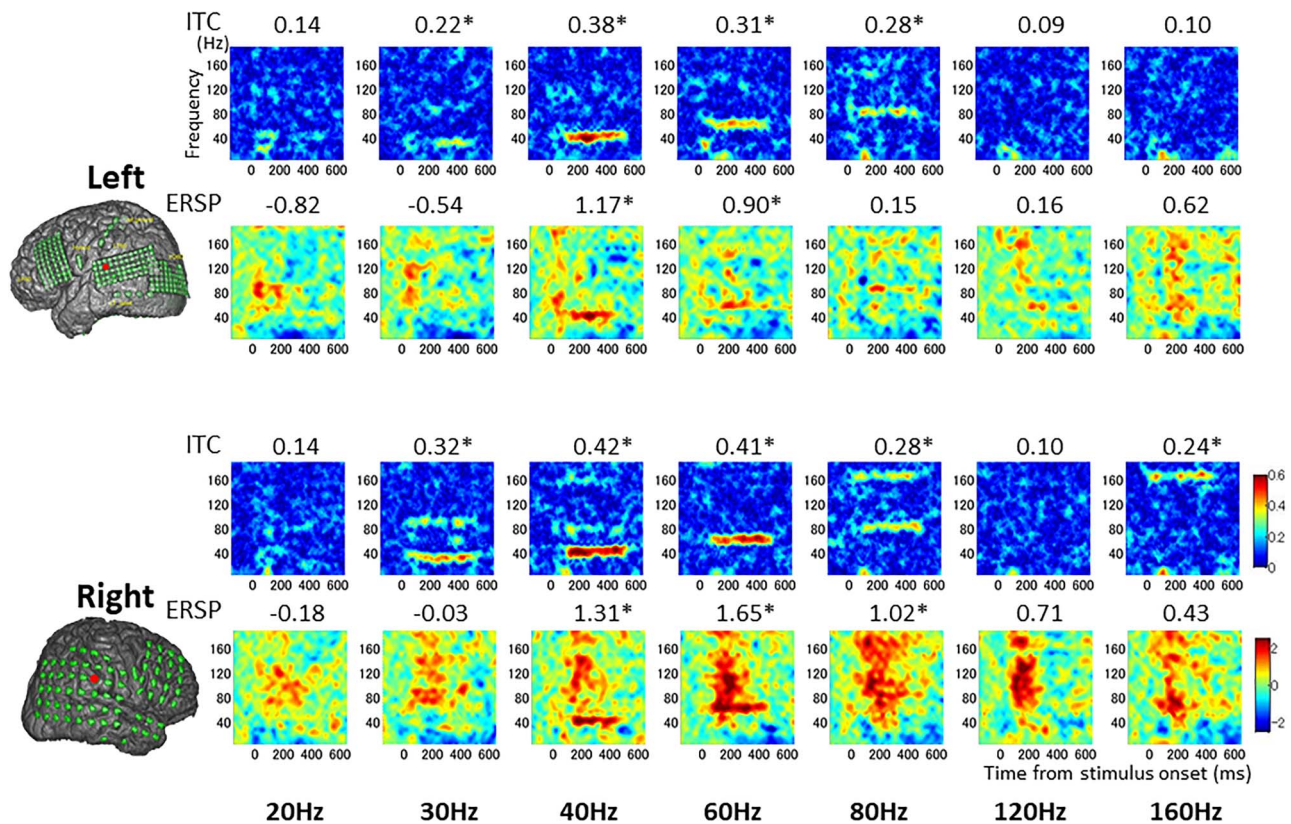


Figure 1. Auditory oscillatory responses are maximized at 40 Hz in the primary auditory cortex (A1). Time-frequency maps of intertrial phase coherence (ITC: first and third row) and (ERSP: second and fourth row) at each stimulus frequency at the electrode (red dot in left insets) closest to A1 in a representative individual (Pt. 1). Top 2 rows indicate the left hemisphere; bottom 2 rows indicate the right hemisphere. In each map, the x-axis indicates time from stimulus onset (ms), and the y-axis indicates frequency (Hz). Color indicates ITC or ERSP at each time frequency point. Numbers above the maps indicate mean ITC/ERSP. Asterisks indicate statistically significant ITC/ERSP.

The ASSR is believed to be composed of an early transient and a late-sustained component, which have different neural underpinnings (Pantev et al. 1993, 1996; Ross et al. 2002; Ross and Pantev 2004; Ding and Simon 2009). Therefore, we analyzed the entire time course of the ASSR and confirmed the presence of transient waveforms in the high-frequency range (80, 120, and 160 Hz). In contrast, sustained responses were apparent in the low-frequency range (30, 40, 60, and 80 Hz). We then calculated the mean ITC for each time block (early: 0–50 ms and late: 150–500 ms).

Statistical Analyses

The significance of ITC values was evaluated by Rayleigh's test, performed using the Matlab CircStat toolbox for circular statistics (Berens 2009) as in Besle et al. (2011). We extracted the angle data at the stimulus frequency for each trial, and tested whether the distribution across trials deviated from random at each time point. The significance of ERSP and HGA values was evaluated using a one-sample t-test. We extracted ERSP at the stimulus frequency, as well as HGA for each trial, and tested whether the distribution across trials deviated from 0 at each time point. ITC, ERSP, and HGA values were considered significant if any P value within 500 ms of the stimulus onset was below 0.01. The false discovery rate (FDR) was controlled using the Benjamini/Hochberg approach. To assess the extent to which evoked power explains ITC/ERSP, we used Spearman's rank correlation coefficient between evoked power and ITC/ERSP.

Frequency selectivity was analyzed using one-way ANOVA by comparing mean ITC values across all electrodes. Subsequently, to elucidate latency-specific ASSR characteristics, a three-way ANOVA (stimuli frequency * time * cortical lobes) was performed. Separate ANOVAs were performed for each hemisphere, because electrode size differed between the left and right. Tukey's honestly significant difference post hoc test was performed for significant main effects. For all ANOVAs, we set the threshold for statistical significance at $P < 0.05$.

All statistical analyses were conducted using custom scripts written in Matlab R2014a (MathWorks).

Results

Auditory Gamma Oscillatory Responses Were Distributed Globally across the Cortex

We measured ASSR using ECoG in 8 patients with refractory epilepsy, using a wide stimulus frequency range (20, 30, 40, 60, 80, 120, and 160 Hz) to elucidate frequency-specific characteristics. We first analyzed the ITC, which measures phase consistency across trials, and the ERSP, which measures relative spectral power compared with baseline, at the electrode closest to A1, which is generally considered to be a main source of ASSR. Figure 1 shows time-frequency maps of ITC and ERSP at each stimulus frequency at one selected electrode near the A1 in a representative individual. Electrode identification was based on visual inspection of the intersection of the lateral sulcus

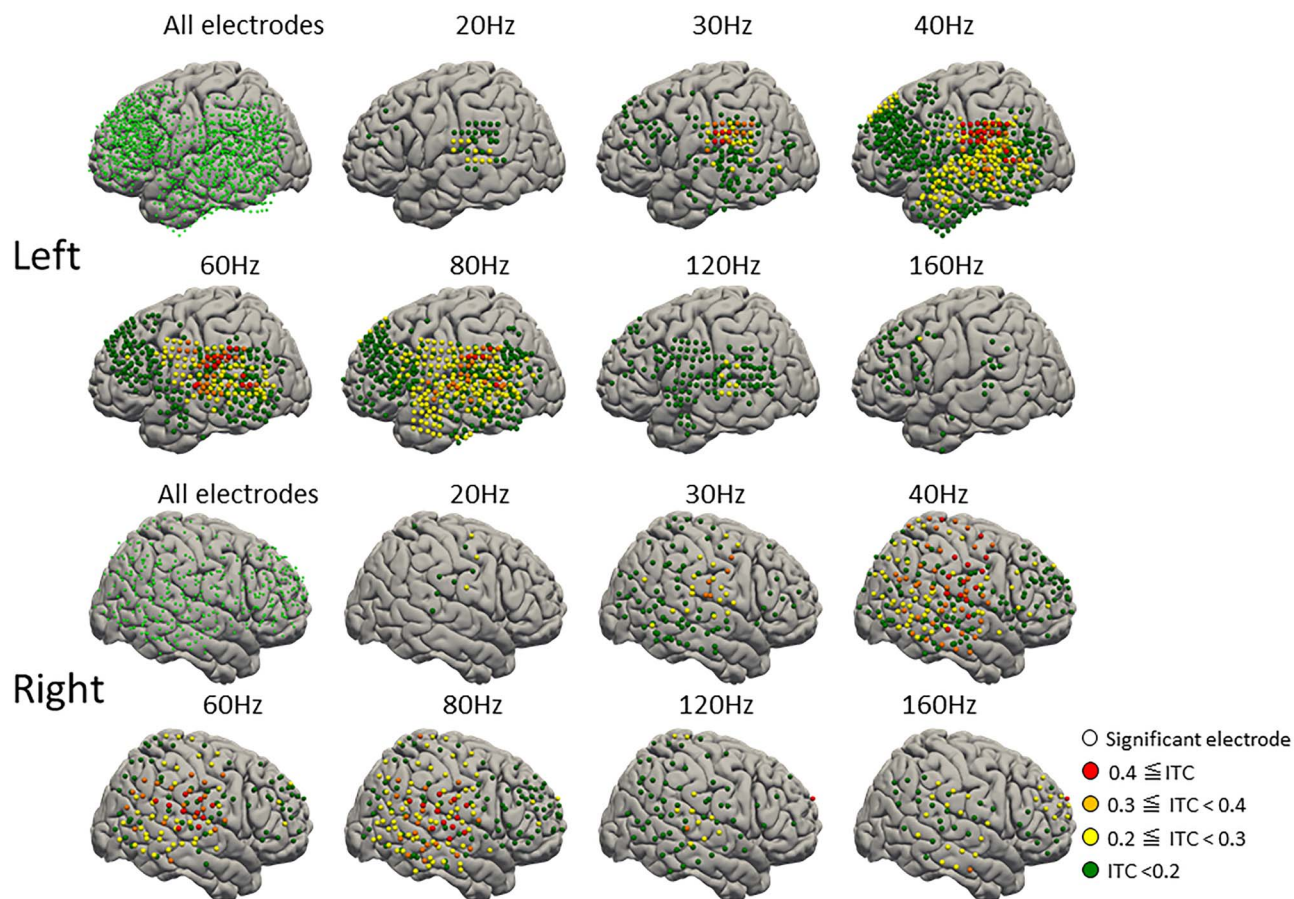


Figure 2. ITC is distributed globally across the cortex. Spatial distribution of electrodes with statistically significant ITCs on the normalized brain for each stimulus frequency. Top 2 rows indicate the left hemisphere; bottom 2 rows indicate the right hemisphere. Electrodes are color-coded depending on the magnitude of ITC.

and a line extending from the postcentral sulcus. Similar to findings from human EEG recordings that ASSR is most evident in the gamma frequency range (30–50 Hz; Galambos et al. 1981; Artieda et al. 2004), robust ITC and ERSP were observed at gamma band stimulus frequencies (30–80 Hz) for both hemispheres. The largest activation within this stimulation frequency range (20–160 Hz) was observed at 40 Hz in the vicinity of A1, which is consistent with the findings of conventional ASSR studies conducted using EEG or MEG. HGA (activity in the high-frequency range that is different from the stimulus frequency in the ERSP map) was also evident, especially in the right hemisphere. HGA was not maximal at 40 Hz, but became stronger with a higher stimulus frequency and was maximal at 120 Hz.

To determine whether the ASSR is localized to A1, we analyzed the spatial distributions of ITC, ERSP, and HGA for all stimulus frequencies combined across all subjects (Figs 2–4). Spatial normalization was performed by extracting MNI coordinates for each electrode. Only electrodes with statistically significant ITC (Rayleigh test, $P < 0.01$, FDR-corrected), ERSP (one-sample t -test, $P < 0.01$, FDR-corrected), and HGA (one-sample t -test, $P < 0.01$, FDR-corrected) values are shown. Interestingly, significant ITC and ERSP values were observed not only near A1 or in the temporal cortex, but also across a wide range of the cortex encompassing the frontal and parietal cortices, particularly at 40-Hz values. HGA was mainly localized near A1, but was still widespread at higher stimulus frequencies.

Finally, we measured evoked power which calculates phase-locked activity. Because evoked power is calculated after averaging across trials, we could not use single-trial values for statistical evaluation. Thus, instead of evaluating the spatial distribution of evoked power, we assessed the correlation between evoked power and ITC/ERSP at 40 Hz. Evoked power was tightly correlated with both ITC and ERSP, but more so with ITC (Fig. 5). The correlation coefficient between evoked power and ITC (Spearman's $r = 0.80$) was greater than that between evoked power and ERSP (Spearman's $r = 0.45$). Therefore, large ITC values were presumably due to activity phase locked to the stimulus.

Auditory Oscillatory Responses Were Maximized at 40 Hz

ITC and ERSP values were maximal at 40 Hz (Fig. 1). To quantify this observation, we examined the average frequency tuning across all electrodes (Fig. 6). A one-way ANOVA of ITC showed a significant main effect of frequency for both the left ($F_{6, 8031} = 210.2$, $P < 0.0001$) and right ($F_{6, 2579} = 72.2$, $P < 0.0001$) hemispheres. ERSP also showed a significant main effect of frequency for both the left ($F_{6, 8031} = 35.1$, $P < 0.0001$) and right ($F_{6, 2579} = 19.5$, $P < 0.0001$) hemispheres. Post-hoc analysis showed that ITC was larger at 40 Hz than at other frequencies in both hemispheres ($P < 0.001$), except at 80 Hz in the right

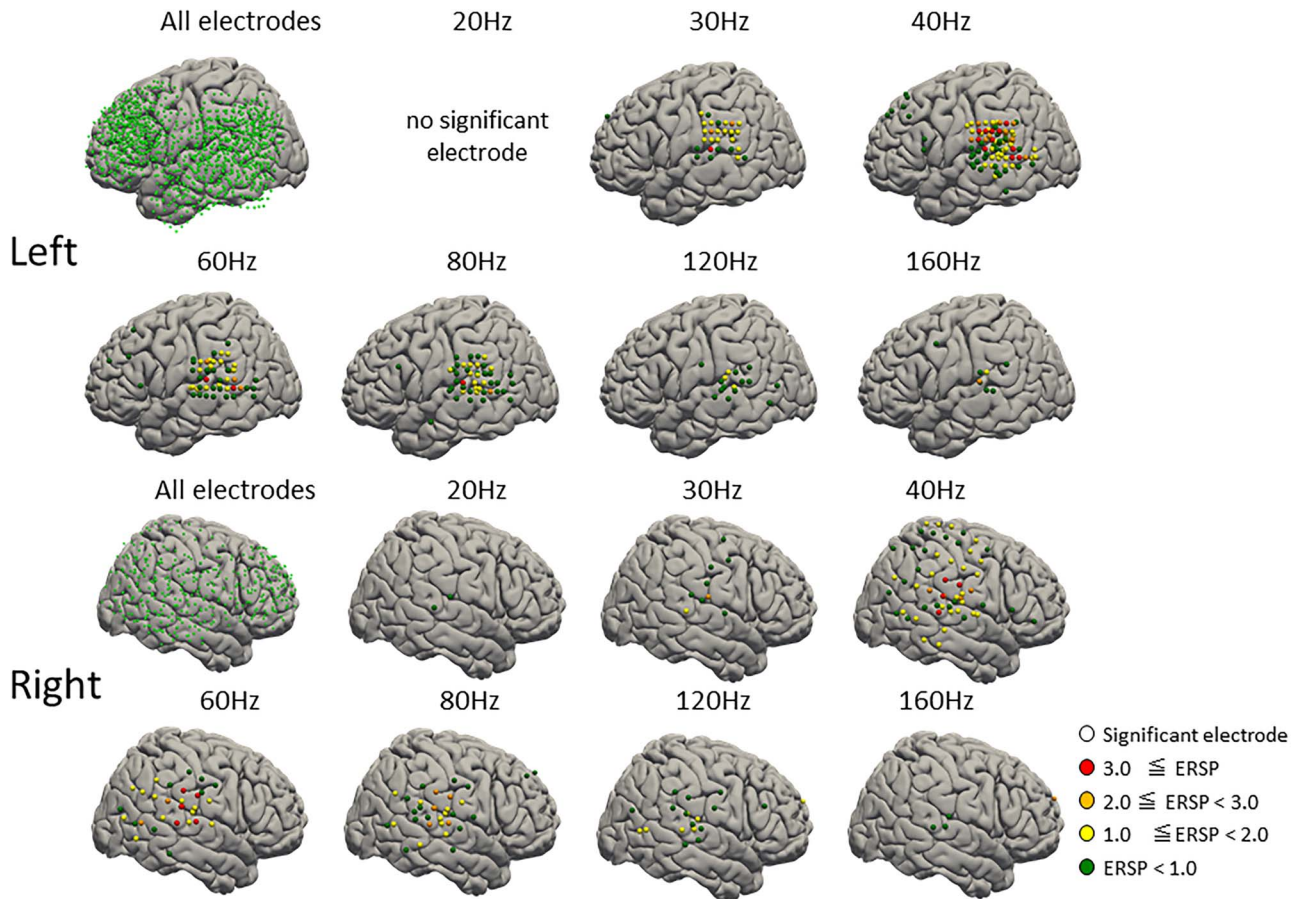


Figure 3. ERSP is distributed globally across the cortex. Spatial distribution of electrodes with statistically significant ERSPs on the normalized brain for each stimulus frequency. Electrodes are color-coded depending on the magnitude of ERSP.

hemisphere ($P=0.99$); ERSP was larger at 40 Hz than at other frequencies in both hemispheres ($P < 0.001$), except for 60 Hz in the right hemisphere ($P=0.91$); these findings are consistent with those of previous EEG studies (Galambos et al. 1981; Artieda et al. 2004). Importantly, ITC was also large among 80-Hz ASSR values, and relatively large among 160-Hz ASSR values. High-frequency ASSRs (> 100 Hz) are known to be difficult to detect using MEG (Pfurtscheller and Cooper 1975; Picton et al. 2003; Hamm et al. 2011), but can be detected using ECoG. Our results revealed that phase synchrony of neural oscillations was maximized not only at 40 Hz, but also at multiples of 40 Hz.

40 Hz ITC Was Prominent in the Parietal, Frontal, and Temporal Cortices

Because ITC was most robust at 40 Hz, we focused our subsequent analysis on 40-Hz ITC values. To further explore the ITC spatial distribution at 40 Hz, we compared ITC values across BA. Each electrode was classified into a BA according to its MNI coordinates using the MNI2TAL conversion tool, a component of the Yale BioImage Suite Package (Papademetris et al., <http://www.bioimagesuite.org>). Figure 7 shows 40-Hz ITC averages across electrodes with statistically significant ITC values (Rayleigh test, $P < 0.01$, FDR corrected) for each BA. A wide distribution of 40-Hz ITC values was observed from the temporal to parietal cortex in the left hemisphere. In the right hemisphere, the frontal cortex

also showed a high frequency of 40-Hz ITC values. Table 2 shows the average ITC (\pm SD) for each BA, as well as the number of electrodes that contributed to the calculation. BA1 (postcentral gyrus) showed the largest ITC, followed by BA40 (supramarginal gyrus) in both hemispheres. This finding confirms that areas in the parietal cortex had the largest ITC values. In the right hemisphere, BA4 (primary motor cortex) and 6 (supplementary motor area) also showed high ITC values. In summary, 40-Hz ITC values were widely distributed throughout the cortex, with the strongest responses seen in the parietal cortex.

Early and Late-Latency Auditory Oscillatory Responses Had Different Frequency Tuning

A recent study showed that the early and late-latency ASSR was impaired differentially at various clinical stages of schizophrenia (Tada et al. 2016). Specifically, an early latency ASSR was reduced in patients with first-episode schizophrenia but intact in a pre-onset ultra-high risk (UHR) group, whereas a late-latency ASSR was reduced in both groups. To determine whether the early and late-latency ASSRs have a different generating mechanism, we first analyzed the time course of the ASSR (Fig. 8). For the high-frequency ASSR (80, 120, and 160 Hz), transient waveforms (a sharp response around 50 ms) were apparent, whereas for the low-frequency ASSR (30, 40, 60, and 80 Hz), sustained responses were apparent. This is consistent

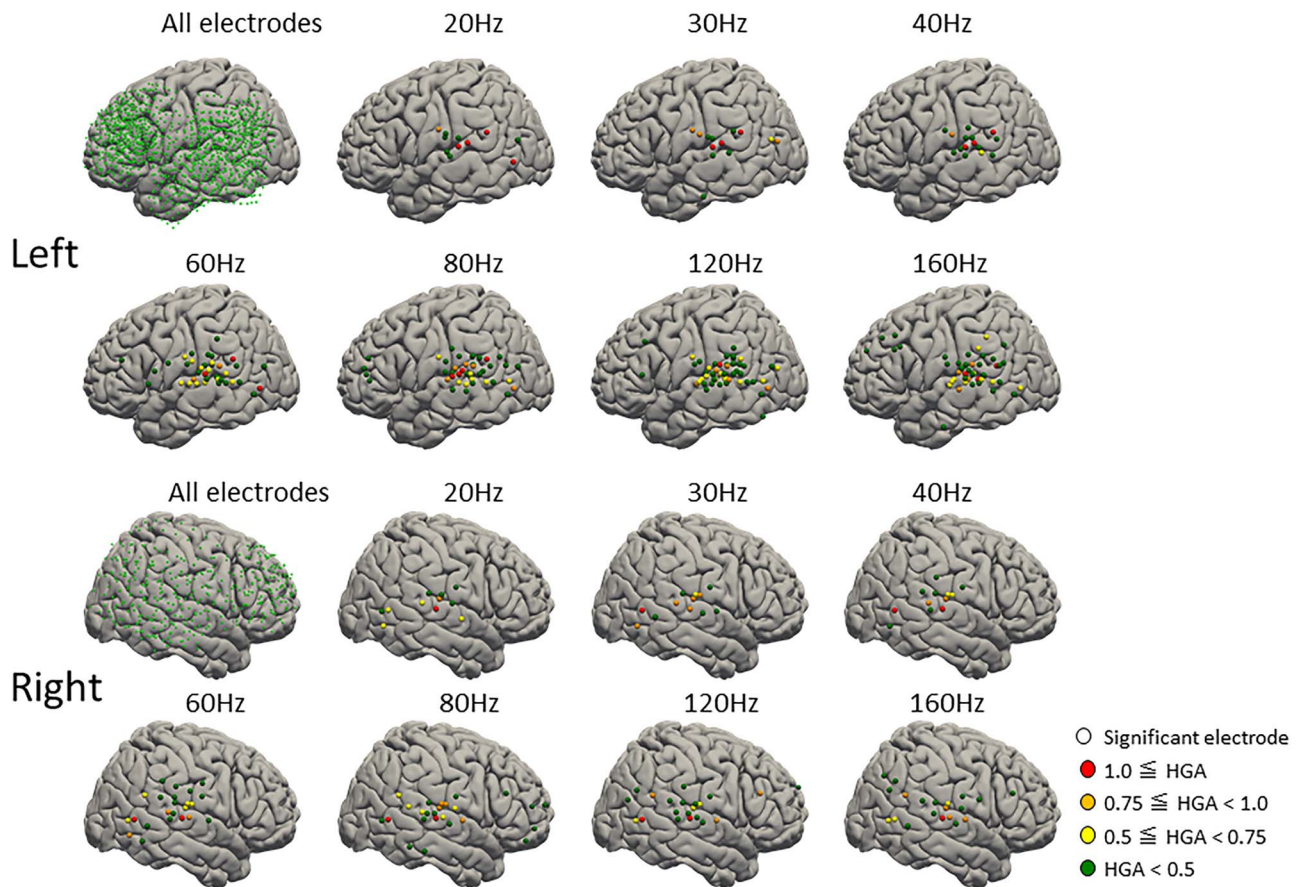


Figure 4. High-gamma activity (HGA) is distributed globally across the cortex. Spatial distribution of electrodes with statistically significant HGAs on the normalized brain for each stimulus frequency. Electrodes are color-coded depending on the magnitude of HGA.

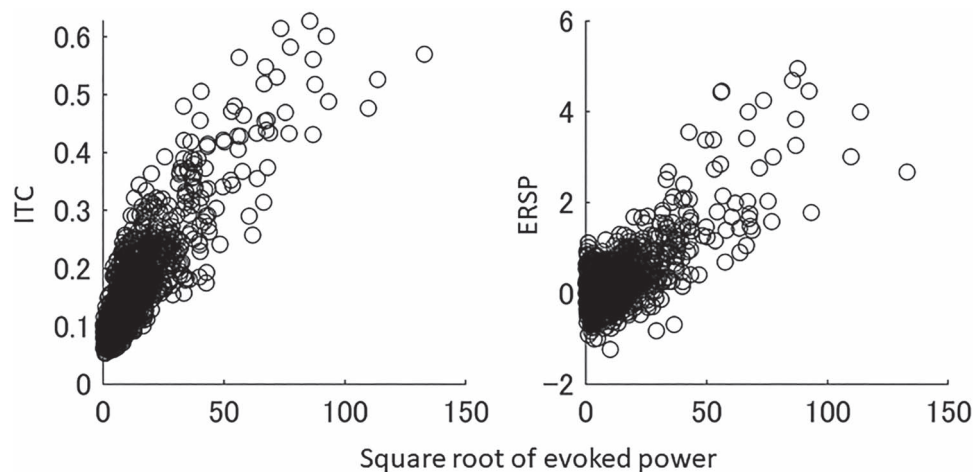


Figure 5. Correlation between evoked power and ITC/ERSP at 40 Hz. Correlation between evoked power and ITC (Left). Correlation between evoked power and ERSP (Right). The abscissa is the square root of evoked power which is equivalent to the ERP amplitude.

with previous studies that proposed that ASSR is composed of a transient and sustained component (Pantev et al. 1993, 1996; Ross et al. 2002; Ross and Pantev 2004; Ding and Simon 2009). The time to peak response depended on the ASSR frequency: the peak latency was shorter for higher frequency stimulation (Figure 9). This suggests that steady-state responses developed

until a certain number of clicks (~ 10) were heard, and were then sustained until the end of auditory stimulation in the case of low-frequency ASSR (30, 40, 60, and 80 Hz).

We next focused our analysis on the frequency tuning of early (0–50 ms) and late- (150–500 ms) latency ASSRs; these time windows were selected so that the overlap between the

Table 2 Number of electrodes and average ITC for each BA in the temporal, parietal, and frontal cortices

Area	BA	No. electrodes (total)		ITC (SD)		Area	BA	No. electrodes (total)		ITC (SD)	
		Left	Right	Left	Right			Left	Right	Left	Right
Frontal	4	8 (11)	8 (12)	0.17 (0.05)	0.27 (0.10)	Parietal	1	14 (24)	13 (15)	0.31 (0.12)	0.31 (0.11)
	6	29 (48)	9 (15)	0.16 (0.03)	0.28 (0.13)		39	57 (176)	24 (43)	0.20 (0.09)	0.21 (0.06)
	8	14 (50)	3 (11)	0.18 (0.06)	0.16 (0.03)		40	46 (81)	27 (40)	0.28 (0.16)	0.30 (0.15)
	9	49 (97)	23 (47)	0.16 (0.04)	0.15 (0.04)	Temporal	20	21 (28)	0 (0)	0.17 (0.03)	
	10	28 (81)	14 (34)	0.15 (0.03)	0.16 (0.03)		21	87 (137)	23 (27)	0.21 (0.07)	0.23 (0.08)
	44	38 (82)	6 (15)	0.16 (0.03)	0.18 (0.05)		22	64 (77)	24 (28)	0.21 (0.06)	0.25 (0.09)
	45	20 (56)	3 (8)	0.15 (0.02)	0.20 (0.09)		37	30 (76)	21 (28)	0.19 (0.04)	0.23 (0.09)
46	19 (63)	2 (11)	0.16 (0.02)	0.14 (0.005)	38	23 (24)	2 (2)	0.19 (0.03)	0.16 (0.04)		
47	7 (20)	3 (8)	0.13 (0.01)	0.17 (0.01)	41 (A1)	20 (22)	6 (7)	0.22 (0.05)	0.23 (0.06)		

Notes: The number of electrodes with significant ITCs is indicated along with the total number of electrodes (in parentheses) for the left and right hemispheres separately. Average ITC for electrodes with statistically significant ITCs are provided along with the SD, separately for the left and right hemispheres.

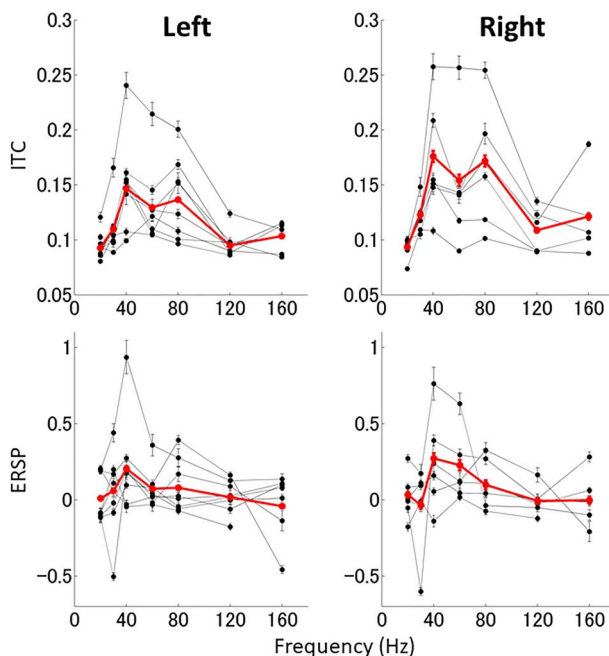


Figure 6. Auditory oscillatory responses are maximized at 40 Hz across the cortex. ITC (top row) and ERSP (bottom row) frequency tuning. Red dots and lines indicate average ITCs and ERSPs across all electrodes in both hemispheres for all individuals. Black dots and dotted lines correspond to frequency tuning for each individual. Error bars indicate SEM across electrodes.

transient and sustained components was minimal. **Figure 10A** shows early and late-latency ITCs at 20- and 40-Hz stimulation for the electrode shown in **Figure 1** (left hemisphere), and **Figure 10B** shows a comparison of early and late-latency ITC magnitude across all electrodes for the same representative individual. At 20 Hz, the magnitude of early latency ITC was comparable with that of late-latency ITC across electrodes (*t*-test, $P=0.94$), whereas the late-latency ITC was much larger than the early latency ITC at 40 Hz (*t*-test, $P < 0.0001$). Thus, the late-latency ITC is robust in the gamma frequency range.

To confirm this finding across subjects and cortical areas, we examined the grand average frequency tuning of the early and

late-latency ITC across all electrodes separately in the temporal, parietal, and frontal lobes (**Fig. 11**). The frequency tuning curve for the early latency ASSR was relatively flat, indicating that frequency selectivity was weak; a modest peak was found at 120 Hz in the right temporal and parietal cortices. By contrast, the frequency tuning curve for the late-latency ASSR peaked significantly at 40 Hz in all parts of the cortex. Three-way ANOVA confirmed the main effects of frequency, area, and latency, as well as interactions among all 3 for the left hemisphere (frequency, $F_{6, 15754} = 186.0$, $P < 0.0001$; area, $F_{2, 15754} = 126.7$, $P < 0.0001$; latency, $F_{1, 15754} = 218.6$, $P < 0.0001$; and all interactions, $P < 0.0001$) and right hemisphere (frequency, $F_{6, 4836} = 79.6$, $P < 0.0001$; area, $F_{2, 4836} = 113.2$, $P < 0.0001$; latency, $F_{1, 4836} = 257.4$, $P < 0.0001$; and all interactions, $P < 0.0001$). A two-way ANOVA performed separately for each area showed main effects of frequency and latency, as well as their interaction for both the left hemisphere (temporal: frequency, $F_{6, 5010} = 88.2$, $P < 0.0001$; latency, $F_{1, 5010} = 120.7$, $P < 0.0001$; interaction, $F_{6, 5010} = 61.1$, $P < 0.0001$; parietal: frequency, $F_{6, 3766} = 37.0$, $P < 0.0001$; latency, $F_{1, 3766} = 60.4$, $P < 0.0001$; interaction, $F_{6, 3766} = 22.5$, $P < 0.0001$; and frontal: frequency, $F_{6, 6978} = 88.8$, $P < 0.0001$; latency, $F_{1, 6978} = 18.6$, $P < 0.0001$; interaction, $F_{6, 6978} = 54.7$, $P < 0.0001$) and the right hemisphere (temporal: frequency, $F_{6, 1242} = 30.1$, $P < 0.0001$; latency, $F_{1, 1242} = 134.0$, $P < 0.0001$; interaction, $F_{6, 1242} = 31.3$, $P < 0.0001$; parietal: frequency, $F_{6, 1416} = 27.6$, $P < 0.0001$; latency, $F_{1, 1416} = 56.7$, $P < 0.0001$; interaction, $F_{6, 1416} = 17.1$, $P < 0.0001$; and frontal: frequency, $F_{6, 2178} = 19.1$, $P < 0.0001$; latency, $F_{1, 2178} = 43.5$, $P < 0.0001$; interaction, $F_{6, 2178} = 9.7$, $P < 0.0001$). Thus, frequency tuning characteristics differed between early and late-latency ASSRs, suggesting different mechanisms for early and late-latency ASSR generation.

Interestingly, frequency tuning for the late-latency ASSR showed a single peak at 40 Hz in the parietal cortex, whereas the temporal and frontal cortices showed double peaks at 40 and 80 Hz for both the left and right hemispheres (**Fig. 11**). A two-way ANOVA performed separately for each latency showed the main effects of frequency and area, as well as their interaction for both the left hemisphere (early: frequency, $F_{6, 7877} = 36.1$, $P < 0.0001$; area, $F_{2, 7877} = 18.2$, $P < 0.0001$; interaction, $F_{12, 7877} = 4.8$, $P < 0.0001$; and late: frequency, $F_{6, 7877} = 284.0$, $P < 0.0001$; area, $F_{2, 7877} = 144.1$, $P < 0.0001$; interaction, $F_{12, 7877} = 20.2$, $P < 0.0001$) and the right hemisphere (early: frequency, $F_{6, 2418} = 20.6$, $P < 0.0001$; area, $F_{2, 2418} = 22.0$,

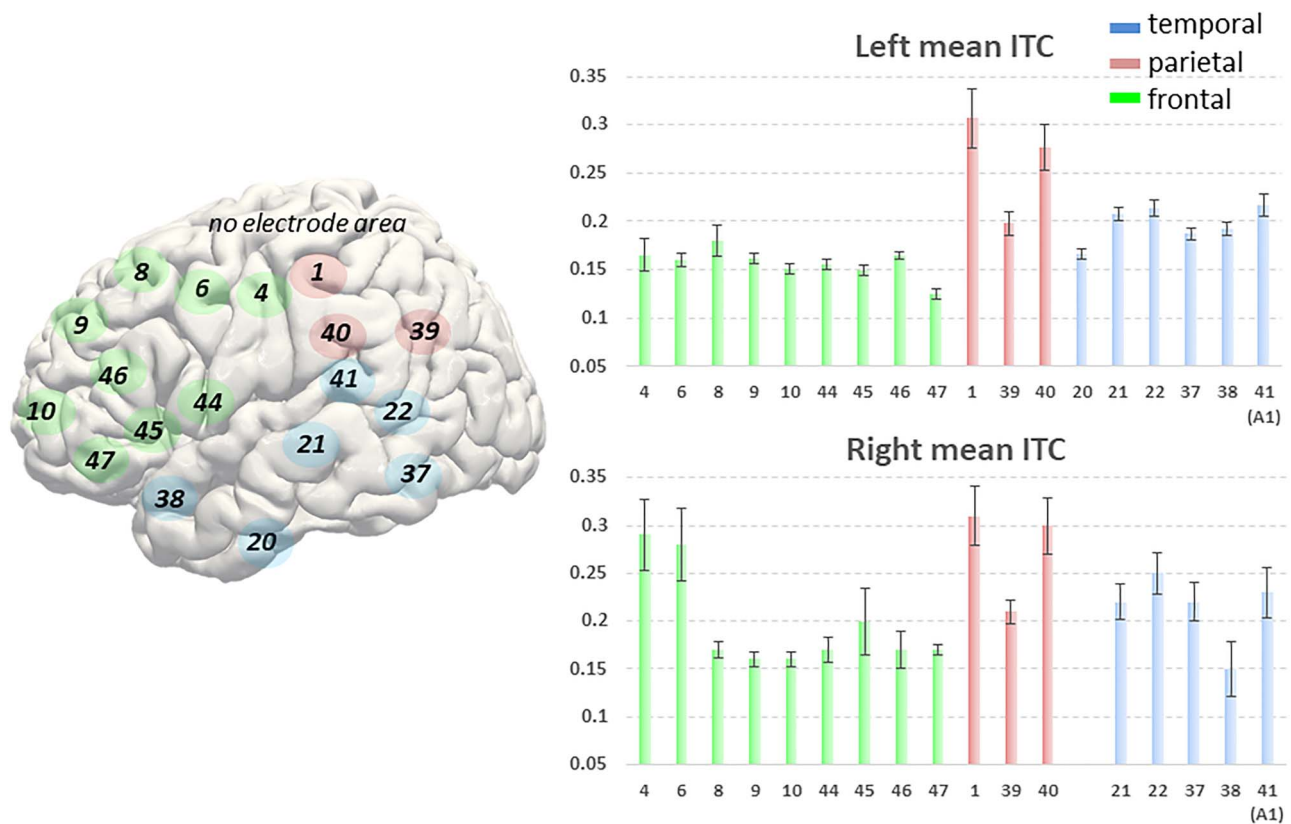


Figure 7. Auditory gamma oscillatory responses in each BA. Average ITC values across electrodes with statistically significant ITCs within each BA in the temporal (blue), parietal (red), and frontal (green) cortices. Error bars indicate standard error of the mean (SEM).

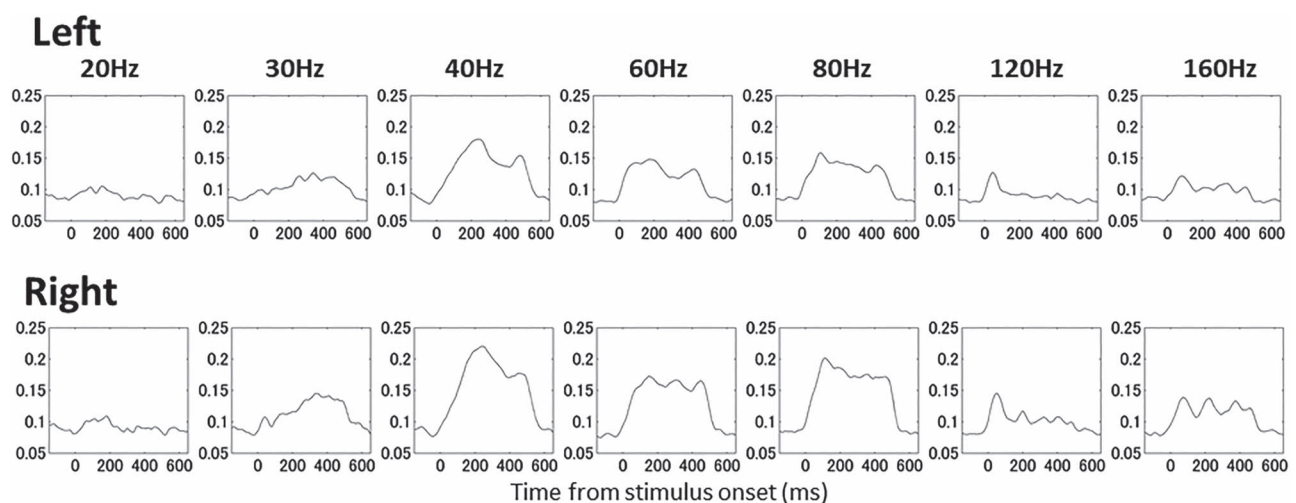


Figure 8. Time course of ITC. The time course of ITC values is shown at each stimulus frequency for the left hemisphere (top row) and right hemisphere (bottom row).

$P < 0.0001$; interaction, $F_{12, 2418} = 2.8$, $P = 0.001$; and late: frequency, $F_{6, 2418} = 110.3$, $P < 0.0001$; area, $F_{2, 2418} = 107.3$, $P < 0.0001$; interaction, $F_{12, 2418} = 13.6$, $P < 0.0001$). Therefore, frequency tuning characteristics of the late-latency ASSR varied between the temporal/frontal and parietal cortex, supporting a differentiation along parallel auditory pathways.

Discussion

In this study, we used ECoG recordings to directly demonstrate that the gamma band ASSR is composed of multiple neural circuits that are widely distributed in the parietal, frontal, and temporal cortices. In particular, we found that frequency tuning characteristics differed between early and late-latency ASSRs.

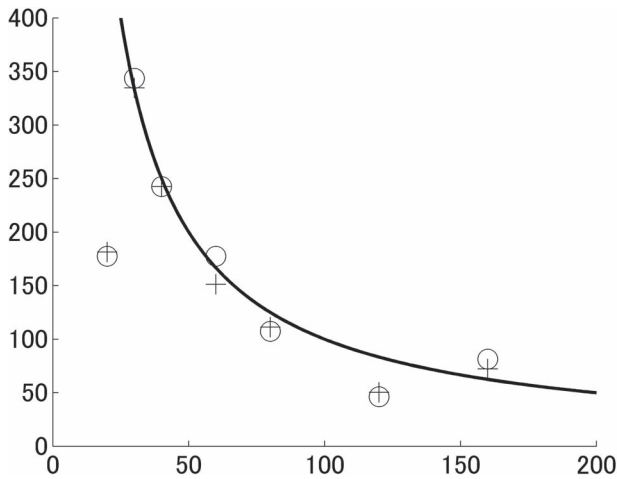


Figure 9. Time to peak ITC depends on the number of tone intervals. Time from tone onset to peak ITC is plotted as a function of stimulus frequency. Circles indicate data from the left hemisphere and crosses indicate data from the right hemisphere. The thick black line indicates the time after 10 stimulus intervals.

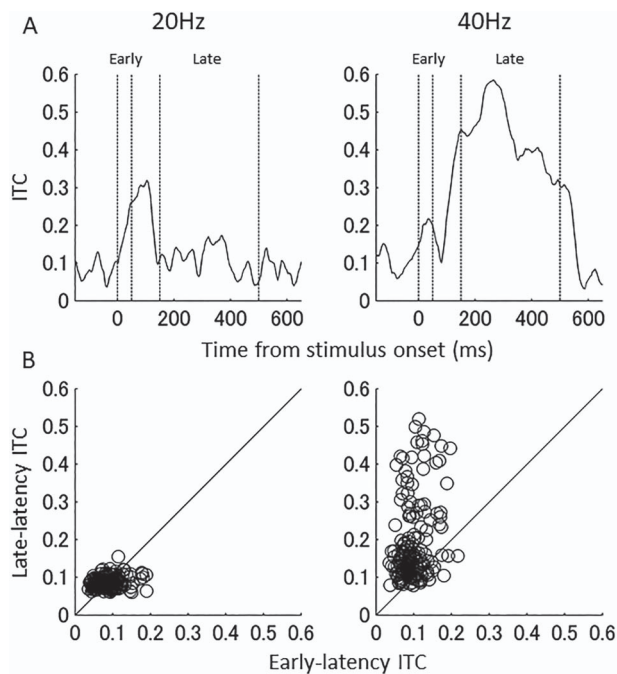


Figure 10. Time course of 40-Hz ITC values is different from that of 20-Hz ITC values. (A) The time course of 20 and 40-Hz ITC values at a representative electrode (as in Fig. 1, left). The x-axis indicates time (ms) and the y-axis indicates ITC. (B) Average late-latency (150–500 ms) ITCs are plotted against average early latency (0–50 ms) ITCs for each electrode in a representative individual (Pt. 1).

Our previous clinical study in patients with schizophrenia showed that early and late-latency ASSRs were differentially impaired between pre-onset UHR individuals and patients with first-episode schizophrenia (Tada et al., 2016). Specifically, the late-latency ASSR was reduced in both groups, whereas the early latency ASSR was intact in the pre-onset UHR group, which is consistent with the suggestion that the ASSR can be decomposed into a transient gamma band response at 0–100 ms, and a steady-state gamma band response at 250–500 ms

(Ross et al., 2002). The present study showed that frequency tuning for the late-latency ASSR was sharper in the gamma frequency range (40 Hz) compared with the weakly tuned early latency ASSR, suggesting that the ASSR consists of the following 2 components: an early broadband response and a late gamma oscillatory response. The former response may simply reflect transient neural firing in response to auditory stimuli, as reported in previous studies (Pantev et al., 1991; Tiitinen et al., 1993), which is weakly dependent on frequency. By contrast, the late response may reflect intrinsic gamma oscillations (Chen et al., 2017).

We also found that the ASSR was widely distributed. In particular, BA1 and BA40 electrodes in the parietal cortex showed the highest ITC values, and frontal areas also showed significant ITCs. These results are in contrast with the conventional view that the ASSR is localized in the auditory cortex (Herdman et al., 2003; Draganova et al., 2008; Brugge et al., 2009). Applying independent component analysis to EEG data, Farahani (2017, 2019) showed widely distributed ASSR sources, located in the cortical and subcortical regions. Specifically, the former study (Farahani et al., 2017) showed that 40 Hz ASSR sources were in the frontal, right limbic, occipital, and left temporal lobes, whereas a later study (Farahani et al., 2019) found sources in the right occipital lobe, precentral gyrus, auditory cortex, and superior parietal lobe. The temporal source was consistent between studies, but the frontal source was not confirmed in the later study. Our present results and another ECoG study (Krom et al., 2020) found ASSRs in both the frontal cortex and temporal cortices. Furthermore, we found parietal ASSRs in addition, to frontal and temporal ones, using chronically implanted electrodes that could detect local signals (Dubey and Ray, 2019). Discrepancies between the findings of the present study and those of previous source estimation studies showing localization in the superior temporal plane may be due to those studies assuming a single or small numbers of sources, as is often the case in MEG studies. Higher signal sensitivity of MEG to brain sulci (e.g., the superior temporal plane) compared with cortical gyri (Cohen and Cuffin, 1983) could also be a confounding factor. The broad distribution observed in this study could have been attributed to volume conduction; however, the distribution was not uniform, which would be predicted by volume conduction. Additionally, volume conduction could not explain the differentiation of frequency tuning between the frontal/temporal and parietal cortices observed in this study. Therefore, we suggest that the ASSR does not originate only in the auditory cortex.

We analyzed the utility of both ITC and ERSP for evaluating ASSRs. ITC had a broader spatial distribution compared with ERSP, likely because ITC and ERSP measure different aspects of ASSR. Indeed, ITC and ERSP show differences in frequency tuning. In addition, the broader distribution of ITC may be due to its greater resiliency to noise. Furthermore, it is possible that gamma-band ITC and ERSP were overestimated because of greater spreading of gamma-band oscillation (Dubey and Ray, 2016). However, in the study of Dubey and Ray (2019), this frequency-dependent spreading was mainly observed for LFP signals and was much weaker for ECoG signals. HGA was stronger and more widespread for higher frequency ASSR. HGA is presumably dependent on auditory stimulus energy and may be different from oscillatory responses.

In addition to its global distribution on the cortical surface, we found significant differences in the frequency tuning characteristics of late gamma oscillatory responses between the parietal and temporal–frontal cortices (Fig. 11): the parietal cortex

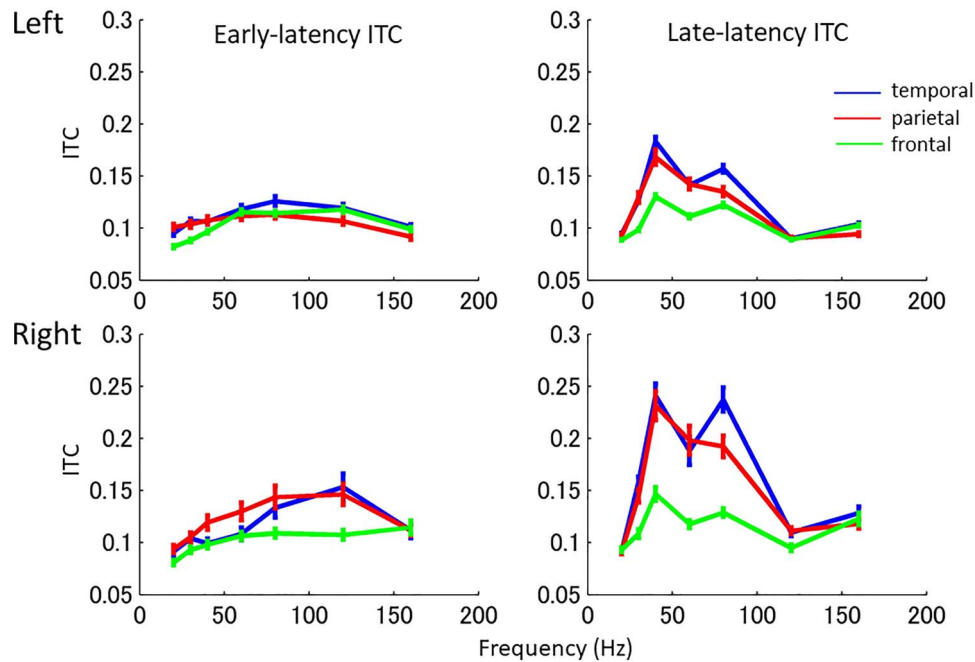


Figure 11. Early and late-latency auditory oscillatory responses have different frequency tuning. Frequency tuning of early and late-latency ITCs. Average ITCs across electrodes was calculated for early (0–50 ms) and late- (150–500 ms) latency ITCs at each stimulus frequency for the temporal (blue), parietal (red), and frontal (green) cortex. Error bars indicate SEM across electrodes.

had a single peak at 40 Hz, whereas the temporal–frontal cortices had double peaks at 40 and 80 Hz. Although the functional relevance of a single peak (40 Hz) in the parietal cortex and double peaks (40 and 80 Hz) in the temporal/frontal cortices remains unclear, the different patterns may arise from local circuits that are tuned to different frequencies in the corresponding lobes, or to the characteristics of the auditory cortex source that project to different lobes via the dorsal and ventral auditory streams (Rauschecker and Scott 2009; Rauschecker 2018). Understanding the bidirectional neural network involved in ASSR generation is an important target for future studies.

Our results suggest that high-gamma oscillations may play a significant role in the temporal–frontal auditory pathway. Interestingly, we found that ITC was large for multiples of 40 Hz; this was not observed for ERSP. We propose that the neural circuits responsible for the generation of ITCs are tuned to 40 Hz, so that the response phase is consistent across trials at 40 Hz, and multiples thereof, compared with other frequencies. Regardless of the underlying mechanism, our findings suggest that ERSP and ITC are dissociable measures of ASSR, and that 40 Hz may be an important index for evaluating oscillatory responses. Previous MEG and ECoG studies have suggested that both high and low (<40 Hz) gamma oscillations are related to various cognitive functions (Crone et al. 2006; Uhlhaas et al. 2011). Some studies have reported that an 80-Hz ASSR is reduced in patients with schizophrenia (Hamm et al. 2011; Tsuchimoto et al. 2011; Puvvada et al. 2018). The neural circuits that underlie differential frequency tuning also remain open for discussion. A previous study reported that both high (> 70 Hz) and low (30–70 Hz) gamma oscillations were dependent on recurrent inhibition; however, their localizations were different in the cat visual cortex (Oke et al. 2010). Oke et al. (2010) found high-gamma oscillations in layer III and low gamma oscillations in

layer V. Although the neural circuit underlying high- and low-gamma oscillation in the human cortex remains unclear, it may be associated with differential distribution of GABAergic interneurons that generate the gamma band.

A reduced gamma band ASSR is robustly detected in neuropsychiatric disorders, especially schizophrenia (Kwon et al. 1999; Light et al. 2006, 2017; Spencer et al. 2008; Brenner et al. 2009; Kirihaara et al. 2012; Thuné et al. 2016). Our findings have several implications for the pathophysiology of neuropsychiatric disorders. We found that the broad distribution of the ASSR was most robust in the gamma band range, which may reflect the resonant activity of gamma oscillations. Abnormal features of gamma band ASSR in neuropsychiatric disorders may reflect brain dysfunction across the cortex, rather than solely reflecting dysfunctions of the auditory cortex. The broad distribution of ASSR may also be related to ASSR attenuation in a variety of psychiatric disorders including autism (Wilson et al. 2007), bipolar disorder (O'Donnell et al. 2004; Rass et al. 2010; Oda et al. 2012), and 22q11.2 deletion syndrome (Larsen et al. 2018). Furthermore, gamma oscillations are considered to be related to the excitation and inhibition (E/I) balance of neurons (Cardin 2016). Moreover, the ASSR is sensitive to the pharmacologic modulation of NMDA receptors in healthy subjects and patients with schizophrenia, which may impact the E/I balance (Light et al. 2017). E/I imbalance is a common pathophysiology in various neuropsychiatric disorders (Tatti et al. 2017). Because the ASSR is not confined to a particular brain area, it may be a useful tool to detect dysfunction in a variety of psychiatric disorders.

Our data show that the ASSR was generally larger in the right hemisphere. Although this finding is consistent with those of previous studies (Ross et al. 2005), our observations should be interpreted with care. The electrode size was larger in the right

hemisphere for all but one patient, which may have resulted in a better signal-to-noise ratio and more coherence among trials.

Our study has several limitations. First, our recordings were conducted in patients with refractory epilepsy. To minimize the effect of the epileptic foci, we performed spatial normalization among 8 participants with differing epileptic foci. Nevertheless, the epileptic foci may have had effects on our results (Matsubara et al. 2018). A recent MEG study reported that ASSRs (phase-locking factor [PLF] and power values) were reduced in patients with mesial temporal lobe epilepsy compared with healthy controls, according to source localization analysis of MEG data for Heschl's gyri (Matsubara et al. 2019). Although our results may not be generalizable to healthy individuals, it seems unlikely that ASSRs were increased by epileptic foci. Second, although the implanted electrodes widely covered the lateral surface of the brain (frontal, parietal, and temporal cortices), areas within the sulci (e.g., superior temporal plane) were not recorded. Because the A1 is embedded in the superior temporal plane, we did not detect responses that directly arose from it. Thus, our evaluation of the relative contributions of superficial cortical areas and the A1 is limited. A previous study (Nourski et al. 2013), which investigated both the lateral temporal lobe and the superior temporal plane showed that both Heschl's gyrus and the posterolateral superior temporal auditory area (posterior portion of the lateral STG) produced ASSRs. Although, larger ASSRs were found in Heschl's gyrus compared with the lateral STG, differences in recording electrodes (ECoG for lateral STG; depth electrode for Heschl's gyrus) may have affected the results. Third, we did not record from subcortical areas. A previous fMRI study demonstrated the contribution of subcortical areas, including the inferior colliculus and the medial geniculate nucleus, to the ASSR (Steinmann and Gutschalk, 2011). Our study did not exclude the contributions of these areas in addition to those of the cerebral cortex. Finally, although subdural ECoG recordings do not require the same kind of spatial reformatting that is often used with scalp EEG (Crone et al. 2006), localization from ECoG is problematic because of the potential influence of volume conduction (Pesaran et al. 2018). Using current source density analysis along with laminar multichannel microelectrodes (Csercsa et al. 2010) may be more useful for precise localization.

In conclusion, we found that the ASSR was distributed globally across the cerebral cortex. Although our results do not preclude the contribution of A1, we suggest that ASSR is generated in a broad range of the cortex, has different generators for time-dependent components, and is communicated in parallel along the temporal/frontal and parietal cortices according to frequency tuning characteristics. Because PV-positive GABAergic interneurons are thought to be crucial for the generation of cortical gamma oscillations (Cardin et al. 2009; Sohal et al. 2009), future studies investigating the differential distribution and abnormalities in cortical GABAergic interneurons across the dual auditory pathway in patients with neuropsychiatric disorders may help to elucidate the pathophysiology underlying the observed ASSR attenuation in patients (Gonzalez-Burgos and Lewis 2008; Fisahn et al. 2009).

Funding

This work was supported in part by grants from the Japan Society for the Promotion of Science (JSPS) KAKENHI (grant 15H06166 and 19K17105 to M.T., 18K07588 to K.K.); Brain Mapping by Integrated Neurotechnologies for Disease Studies (Brain/MINDS)

of the Japan Agency for Medical Research and Development (AMED) (grant 17dm0207004h0004, JP20dm0207069 to N.K., T.U., and K.K.); the International Research Center for Neurointelligence (WPI-IRCN) at The University of Tokyo Institutes for Advanced Study (UTIAS) to M.T. and K.K.; University of Tokyo Center for Integrative Science of Human Behavior (CiSHuB) to K.K.; the Takeda Science Foundation to M.T., the Naito Foundation to M.T. and Kurata Grants to M.T.

Notes

Conflict of Interest: The authors declare no competing interests.

Authors' Contributions

M.T., K.K., Y.I., N.K., and K.K. designed the study. M.T., Y.I., N.K., S.S., K.I., D.K., and M.F. collected the data. M.T., K.K., Y.I., M.T., N.K., and T.U. analyzed the data. M.T., K.K., Y.I., M.T., N.K., T.U., S.S., D.K., M.F., T.A., and K.K. interpreted the results. M.T., K.K., Y.I., N.K., T.U., and K.K. wrote the manuscript. K.K., N.S., and K.K. supervised all aspects of data collection, analysis, and interpretation.

References

- Artieda J, Valencia M, Alegre M, Olaziregi O, Urrestarazu E, Iriarte J. 2004. Potentials evoked by chirp-modulated tones: a new technique to evaluate oscillatory activity in the auditory pathway. *Clin Neurophysiol.* 115:699–709.
- Berens P. 2009. CircStat: a MATLAB toolbox for circular statistics. *J Stat Softw.* 31:1–21.
- Besle J, Schevon CA, Mehta AD, Lakatos P, Goodman RR, McKhann GM, Emerson RG, Schroeder CE. 2011. Tuning of the human neocortex to the temporal dynamics of attended events. *J Neurosci.* 31:3176–3185.
- Brenner CA, Krishnan GP, Vohs JL, Ahn WY, Hetrick WP, Morzorati SL, O'Donnell BF. 2009. Steady state responses: electrophysiological assessment of sensory function in schizophrenia. *Schizophr Bull.* 35:1065–1077.
- Brugge JF, Noursli KV, Oya H, Reale RA, Kawasaki H, Stein-schneider M, Howard MA 3rd. 2009. Coding of repetitive transients by auditory cortex on Heschl's gyrus. *J Neurophysiol.* 102:2358–2374.
- Cardin JA, Carlen M, Meletis K, Knoblich U, Zhang F, Deisseroth K, Tsai LH, Moore CI. 2009. Driving fast-spiking cells induces gamma rhythm and controls sensory responses. *Nature.* 459:663–667.
- Cardin JA. 2016. Snapshots of the brain in action: local circuit operations through the lens of γ oscillations. *J Neurosci.* 36:10496–10504.
- Chen G, Zhang Y, Li X, Zhao X, Ye Q, Lin Y, Tao HW, Rasch MJ, Zhang X. 2017. Distinct inhibitory circuits orchestrate cortical beta and gamma band oscillations. *Neuron.* 20:1403–1418.
- Cohen D, Cuffin BN. 1983. Demonstration of useful differences between magnetoencephalogram and electroencephalogram. *Electroencephalogr Clin Neurophysiol.* 56:38–51.
- Crone NE, Sinai A, Korzeniewska A. 2006. High-frequency gamma oscillations and human brain mapping with electrocorticography. *Prog Brain Res.* 159:275–295.
- Csercsa R, Dombovári B, Fabó D, Wittner L, Eross L, Entz L, Sólyom A, Rásonyi G, Szucs A, Kelemen A, et al. 2010. Laminar analysis of slow wave activity in humans. *Brain.* 133:2814–2829.

- Delorme A, Makeig S. 2004. EEGLAB: an open source toolbox for analysis of single-trial EEG dynamics including independent component analysis. *J Neurosci Methods*. 134:9–21.
- Ding N, Simon JZ. 2009. Neural representations of complex temporal modulations in the human auditory cortex. *J Neurophysiol*. 102:2731–2743.
- Draganova R, Ross B, Wollbrink A, Pantev C. 2008. Cortical steady-state responses to central and peripheral auditory beats. *Cereb Cortex*. 15:1193–1200.
- Dubey A, Ray S. 2016. Spatial spread of local field potential is band-pass in the primary visual cortex. *J Neurophysiol*. 116:1986–1999.
- Dubey A, Ray S. 2019. Cortical electrocorticogram (ECoG) is a local signal. *J Neurosci*. 39(22):4299–4311.
- Farahani ED, Goossens T, Wouters J, Wieringen A. 2017. Spatiotemporal reconstruction of auditory steady-state responses to acoustic amplitude modulations: potential sources beyond the auditory pathway. *Neuroimage*. 148:240–253.
- Farahani ED, Wouters J, Wieringen A. 2019. Contributions of non-primary cortical sources to auditory temporal processing. *Neuroimage*. 191:303–314.
- Fisahn A, Neddens J, Yan L, Buonanno A. 2009. Neuregulin-1 modulates hippocampal gamma oscillations: implications for schizophrenia. *Cereb Cortex*. 19:612–618.
- Galambos R, Makeig S, Tarmachoff PJ. 1981. A 40-Hz auditory potential recorded from the human scalp. *Proc Natl Acad Sci U S A*. 78:2643–2647.
- Gonzalez-Burgos G, Lewis DA. 2008. GABA neurons and the mechanisms of network oscillations: implications for understanding cortical dysfunction in schizophrenia. *Schizophr Bull*. 34:944–961.
- Hamm JP, Gilmore CS, Picchetti NA, Sponheim SR, Clementz BA. 2011. Abnormalities of neuronal oscillations and temporal integration to low- and high-frequency auditory stimulation in schizophrenia. *Biol Psychiatry*. 69:989–996.
- Herdman AT, Wollbrink A, Chau W, Ishii R, Ross B, Pantev C. 2003. Determination of activation areas in the human auditory cortex by means of synthetic aperture magnetometry. *Neuroimage*. 20:995–1005.
- Hutcheon B, Yarom Y. 2000. Resonance, oscillation, and the intrinsic frequency preferences of neurons. *Trends Neurosci*. 23:216–222.
- Ishishita Y, Kunii N, Shimada S, Ibayashi K, Tada M, Kirihara K, Kawai K, Uka T, Kasai K, Saito N. 2019. Deviance detection is the dominant component of auditory contextual processing in the lateral superior temporal gyrus: a human ECoG study. *Hum Brain Mapp*. 40:1184–1194.
- Kirihara K, Rissling AJ, Swerdlow NR, Braff DL, Light GA. 2012. Hierarchical organization of gamma and theta oscillatory dynamics in schizophrenia. *Biol Psychiatry*. 71:873–880.
- Kopell N, Kramer MA, Malerba P, Whittington MA. 2010. Are different rhythms good for different functions? *Front Hum Neurosci*. 4:187.
- Koshiyama D, Kirihara K, Tada M, Nagai T, Fujioka M, Ichikawa E, Ohta K, Tani M, Tsuchiya M, Kanehara A, et al. 2018. Auditory gamma oscillations predict global symptomatic outcome in the early stages of psychosis: a longitudinal investigation. *Clin Neurophysiol*. 129:2268–2275.
- Kozono N, Honda S, Tada M, Kirihara K, Zhao Z, Jinde S, Uka T, Yamada H, Matsumoto M, Kasai K, et al. 2019. Auditory steady state response; nature and utility as a translational science tool. *Sci Rep*. 9:8454. doi: [10.1038/s41598-019-44936-3](https://doi.org/10.1038/s41598-019-44936-3).
- Krom AJ, Marmelshtein A, Gelbard-Sagiv H, Tankus A, Hayat H, Hayat D, Matot I, Strauss I, Fahoum F, Soehle M, et al. 2020. Anesthesia-induced loss of consciousness disrupts auditory responses beyond primary cortex. *Proc Natl Acad Sci U S A*. 117:11770–11780.
- Kunii N, Kamada K, Ota T, Greenblatt RE, Kawai K, Saito N. 2013a. The dynamics of language-related high-gamma activity assessed on a spatially-normalized brain. *Clin Neurophysiol*. 124:91–100.
- Kunii N, Kamada K, Ota T, Kawai K, Saito N. 2013b. Characteristic profiles of high gamma activity and blood oxygenation level-dependent responses in various language areas. *Neuroimage*. 65:242–249.
- Kwon JS, O'Donnell BF, Wallenstein GV, Greene RW, Hirayasu Y, Nestor PG, Hasselmo ME, Potts GF, Shenton ME, McCarley RW. 1999. Gamma frequency-range abnormalities to auditory stimulation in schizophrenia. *Arch Gen Psychiatry*. 56:1001–1005.
- Lacadie CM, Fulbright RK, Constable RT, Papademetris X. 2008. More accurate Talairach coordinates for neuroimaging using nonlinear registration. *Neuroimage*. 42:717–725.
- Larsen KM, Pellegrino G, Birknow MR, Kjær TN, Baaré WFC, Didriksen M, Olsen L, Werge T, Mørup M, Siebner HR. 2018. 22q11.2 deletion syndrome is associated with impaired auditory steady-state gamma response. *Schizophr Bull*. 44:388–397.
- Light GA, Hsu JL, Hsieh MH, Meyer-Gomes K, Sprock J, Swerdlow NR, Braff DL. 2006. Gamma band oscillations reveal neural network cortical coherence dysfunction in schizophrenia patients. *Biol Psychiatry*. 60:1231–1240.
- Light GA, Zhang W, Joshi YB, Bhakta S, Talledo JA, Swerdlow NR. 2017. Single-dose memantine improves cortical oscillatory response dynamics in patients with schizophrenia. *Neuropsychopharmacology*. 42:2633–2639.
- Matsubara T, Ogata K, Hironaga N, Kikuchi Y, Uehara T, Chatani H, Mitsudo T, Shigeto H, Tobimatsu S. 2018. Altered neural synchronization to pure-tone stimulation in patients with mesial temporal lobe epilepsy: an MEG study. *Epilepsy Behav*. 88:96–105.
- Matsubara T, Ogata K, Hironaga N, Uehara T, Mitsudo T, Shigeto H, Maekawa T, Tobimatsu S. 2019. Monaural 40-Hz auditory steady-state magnetic responses can be useful for identifying epileptic focus in mesial temporal lobe epilepsy. *Clin Neurophysiol*. 130:341–351.
- Nourski KV, Brugge JF, Reale RA, Kovach CK, Oya H, Kawasaki H, Jenison RL, Howard MA 3rd. 2013. Coding of repetitive transients by auditory cortex on posterolateral superior temporal gyrus in humans: an intracranial electrophysiology study. *J Neurophysiol*. 109:1283–1295.
- Oda Y, Onitsuka T, Tsuchimoto R, Hirano S, Oribe N, Ueno T, Hirano Y, Nakamura I, Miura T, Kanba S. 2012. Gamma band neural synchronization deficits for auditory steady state responses in bipolar disorder patients. *PLoS One*. 7:e39955.
- O'Donnell BF, Hetrick WP, Vohs JL, Krishnan GP, Carroll CA, Shekhar A. 2004. Neural synchronization deficits to auditory stimulation in bipolar disorder. *Neuroreport*. 15:1369–1372.
- Oke OO, Magony A, Anver H, Ward PD, Jiruska P, Jefferys JG, Vreugdenhil M. 2010. High-frequency gamma oscillations coexist with low-frequency gamma oscillations in the rat visual cortex in vitro. *Eur J Neurosci*. 31:1435–1445.
- Pantev C, Makeig S, Hoke M, Galambos R, Hampson S, Gallen C. 1991. Human auditory evoked gamma-band magnetic fields. *Proc Natl Acad Sci U S A*. 88:8996–9000.

- Pantev C, Elbert T, Makeig S, Hampson S, Eulitz C, Hoke M. 1993. Relationship of transient and steady-state auditory evoked fields. *Electroencephalogr Clin Neurophysiol.* 88(5):389–396.
- Pantev C, Roberts LE, Elbert T, Ross B, Wienbruch C. 1996. Tonic organization of the sources of human auditory steady-state responses. *Hear Res.* 101:62–74.
- Pesaran B, Vinck M, Einevoll GT, Sirota A, Fries P, Siegel M, Truccolo W, Schroeder CE, Srinivasan R. 2018. Investigating large-scale brain dynamics using field potential recordings: analysis and interpretation. *Nat Neurosci.* 21:903–919.
- Pfurtscheller G, Cooper R. 1975. Frequency dependence of the transmission of the EEG from cortex to scalp. *Electroencephalogr Clin Neurophysiol.* 38:93–96.
- Picton TW, John MS, Dimitrijevic A, Purcell D. 2003. Human auditory steady-state responses. *Int J Audiol.* 42:177–219.
- Puvvada KC, Summerfelt A, Du X, Krishna N, Kochunov P, Rowland LM, Simon JZ, Hong LE. 2018. Delta vs. gamma auditory steady state synchrony in schizophrenia. *Schizophr Bull.* 15:378–387.
- Rass O, Krishnan G, Brenner CA, Hetrick WP, Merrill CC, Shekhar A, O'Donnell BF. 2010. Auditory steady state response in bipolar disorder: relation to clinical state, cognitive performance, medication status, and substance disorders. *Bipolar Disord.* 12:793–803.
- Rauschecker JP, Scott SK. 2009. Maps and streams in the auditory cortex: nonhuman primates illuminate human speech processing. *Nat Neurosci.* 12:718–724.
- Rauschecker JP. 2018. Where, when, and how: are they all sensorimotor? Towards a unified view of the dorsal pathway in vision and audition. *Cortex.* 98:262–268.
- Ray S, Crone NE, Niebur E, Franaszczuk PJ, Hsiao SS. 2008. Neural correlates of high-gamma oscillations (60–200 Hz) in macaque local field potentials and their potential implications in electrocorticography. *J Neurosci.* 28:11526–11536.
- Roach BJ, Mathalon DH. 2008. Event-related EEG time-frequency analysis: an overview of measures and an analysis of early gamma band phase locking in schizophrenia. *Schizophr Bull.* 34:907–926.
- Rojas DC, Teale PD, Maharajh K, Kronberg E, Youngpeter K, Wilson LB, Wallace A, Hepburn S. 2011. Transient and steady-state auditory gamma-band responses in first-degree relatives of people with autism spectrum disorder. *Mol Autism.* 2:11.
- Ross B, Picton TW, Pantev C. 2002. Temporal integration in the human auditory cortex as represented by the development of the steady-state magnetic field. *Hear Res.* 165:68–84.
- Ross B, Pantev C. 2004. Auditory steady-state responses reveal amplitude modulation gap detection thresholds. *J Acoust Soc Am.* 115:2193–2206.
- Ross B, Herdman AT, Pantev C. 2005. Right hemispheric laterality of human 40 Hz auditory steady-state responses. *Cereb Cortex.* 15:2029–2039.
- Sheehan DV, Lecrubier Y, Sheehan KH, Amorim P, Janavs J, Weiller E, Hergueta T, Baker R, Dunbar GC. 1998. The mini-international neuropsychiatric interview (M.I.N.I.): the development and validation of a structured diagnostic psychiatric interview for DSM-IV and ICD-10. *J Clin Psychiatry.* 59:22–33 quiz 34–57.
- Sivarao DV. 2015. The 40-Hz auditory steady-state response: a selective biomarker for cortical NMDA function. *Ann N Y Acad Sci.* 1344:27–36.
- Sivarao DV, Chen P, Senapati A, Yang Y, Fernandes A, Benitez Y, Whiterock V, Li YW, Ahlijanian MK. 2016. 40 Hz auditory steady-state response is a pharmacodynamic biomarker for cortical NMDA receptors. *Neuropsychopharmacology.* 41:2232–2240.
- Sohal VS, Zhang F, Yizhar O, Deisseroth K. 2009. Parvalbumin neurons and gamma rhythms enhance cortical circuit performance. *Nature.* 459:698–702.
- Spencer KM, Salisbury DF, Shenton ME, McCarley RW. 2008. Gamma-band auditory steady-state responses are impaired in first episode psychosis. *Biol Psychiatry.* 64:369–375.
- Steinmann I, Gutschalk A. 2011. Potential fMRI correlates of 40-Hz phase locking in primary auditory cortex, thalamus and midbrain. *Neuroimage.* 1:495–504.
- Sun Y, Farzan F, Barr MS, Kirihara K, Fitzgerald PB, Light GA, Daskalakis ZJ. 2011. γ oscillations in schizophrenia: mechanisms and clinical significance. *Brain Res.* 1413:98–114.
- Tada M, Nagai T, Kirihara K, Koike S, Suga M, Araki T, Kobayashi T, Kasai K. 2016. Differential alterations of auditory gamma oscillatory responses between pre-onset high-risk individuals and first-episode schizophrenia. *Cereb Cortex.* 26:1027–1035.
- Tada M, Kirihara K, Koshiyama D, Fujioka M, Usui K, Uka T, Komatsu M, Kunii N, Araki T, Kasai K. 2019. Gamma-band auditory steady-state response as a neurophysiological marker for excitation and inhibition balance: a review for understanding schizophrenia and other neuropsychiatric disorders. *Clin EEG Neurosci.* 51:234–243. doi: [10.1177/1550059419868872](https://doi.org/10.1177/1550059419868872).
- Takasago M, Kunii N, Komatsu M, Tada M, Kirihara K, Uka T, Ishishita Y, Shimada S, Kasai K, Saito N. 2020. Spatiotemporal differentiation of MMN from N1 adaptation: a human ECoG study. *Front Psych.* 11:586.
- Tatti R, Haley MS, Swanson OK, Tselha T, Maffei A. 2017. Neurophysiology and regulation of the balance between excitation and inhibition in neocortical circuits. *Biol Psychiatry.* 15:821–831.
- Thuné H, Recasens M, Uhlhaas PJ. 2016. The 40-Hz auditory steady-state response in patients with schizophrenia. A meta-analysis. *JAMA Psychiat.* 73:1145–1153.
- Tiitinen H, Sinkkonen J, Reinikainen K, Alho K, Lavikainen J, Näätänen R. 1993. Selective attention enhances the auditory 40-Hz transient response in humans. *Nature.* 364:59–60.
- Tsushima R, Kanba S, Hirano S, Oribe N, Ueno T, Hirano Y, Nakamura I, Oda Y, Miura T, Onitsuka T. 2011. Reduced high and low frequency gamma synchronization in patients with chronic schizophrenia. *Schizophr Res.* 133:99–105.
- Uhlhaas PJ, Singer W. 2010. Abnormal neural oscillations and synchrony in schizophrenia. *Nat Rev Neurosci.* 11:100–113.
- Uhlhaas PJ, Pipa G, Neunenschwander S, Wibral M, Singer W. 2011. A new look at gamma? High- (>60 Hz) γ -band activity in cortical networks: function, mechanisms and impairment. *Prog Biophys Mol Biol.* 105:14–28.
- Wilson TW, Rojas DC, Reite ML, Teale PD, Rogers SJ. 2007. Children and adolescents with autism exhibit reduced MEG steady-state gamma responses. *Biol Psychiatry.* 62:192–197.
- Wilson TW, Hernandez OO, Asherin RM, Teale PD, Reite ML, Rojas DC. 2008. Cortical gamma generators suggest abnor-

- mal auditory circuitry in early-onset psychosis. *Cereb Cortex*. 18:371–378.
- Whittington MA, Traub RD, Adams NE. 2019. A future for neuronal oscillation research. *Brain Neurosci Adv*. 2:2398212818794827. doi: [10.1177/2398212818794827](https://doi.org/10.1177/2398212818794827).
- Zhou TH, Mueller NE, Spencer KM, Mallya SG, Lewandowski KE, Norris LA, Levy LD, Cohen BM, Öngür D, Hall MH. 2018. Auditory steady state response deficits are associated with symptom severity and poor functioning in patients with psychotic disorder. *Schizophr Res*. 201:278–286.